



ARTICLE

An Experimental Investigation on Workability and Bleeding Behaviors of Cement Pastes Doped with Nano Titanium Oxide (n-TiO₂) Nanoparticles and Fly Ash

Fatih Çelik^{1,*}, Oğuzhan Yıldız², Andaç Batur Çolak³ and Samet Mufit Bozkır¹

¹Civil Engineering Department, Niğde Ömer Halisdemir University, Niğde, Turkey

²Electric and Energy Department, Niğde Ömer Halisdemir University, Niğde, Turkey

³Mechanical Engineering Department, Niğde Ömer Halisdemir University, Niğde, Turkey

*Corresponding Author: Fatih Çelik. Email: fatihcelik@ohu.edu.tr

Received: 23 December 2021 Accepted: 26 March 2022

ABSTRACT

In this study, the workability of cement-based grouts containing n-TiO₂ nanoparticles and fly ash has been investigated experimentally. Several characteristic quantities (including, but not limited to, the marsh cone flow time, the mini slump spreading diameter and the plate cohesion meter value) have been measured for different percentages of these additives. The use of fly ash as a mineral additive has been found to result in improvements in terms of workability behavior as expected. Moreover, if nano titanium oxide is also used, an improvement can be obtained regarding the bleeding values for the cement-based grout mixes. Using such experimental data, a multi-layer perceptron artificial neural network model has been developed (5 neurons in the hidden layer of the network model have been developed using a total of 42 experimental data). 70% of the data employed in this model have been used for training, 15% for validation and 15% for the test phase. The results demonstrate that the artificial neural network model can predict Marsh cone flow time, mini slump spreading diameter and plate cohesion meter values with an average error of 0.15%.

KEYWORDS

Nano titanium oxide; fly ash; workability of grouts; bleeding; stability of grouts; ANN

1 Introduction

Due to the recent developments in nano technology, the use of nano powders as additives in cement-based mixtures has become widespread. Some previous studies presented have shown that the use of nano powders as additives in cement-based grouts has improved some of the mechanical and workability properties of fresh grout mixes [1]. These past studies have shown that by using nano powders as additives, properties such as rheological, workability and durability can be improved as well as the hardened properties of cement-based grouts [2,3]. The most widely used material as nano additive in cement-based grouts is nano silica in the past studies. In these studies, it has been shown that the use of nano silica as an additive in cement-based grouts increases hydration products and reduces the setting times of fresh grout samples [4–6]. In addition, it has been shown in other studies that the use of nano silica in concrete mixtures improves the porous structure of hardened concrete by closing the voids [7,8].



The fact that such nano materials have a large specific surface area due to their nanoscale dimensions has increased the water requirement of the mixtures when they are added as an additive to cement based grout mixes [9,10]. Ouyang et al. [11] showed that the use of nano silica as an additive in cement-based grouts with different water binding ratios (w/b) significantly affects the apparent viscosity values of these grout mixtures. With this experimental study, they presented a new analytical prediction model to predict the viscosity behavior of grout mixes. The effects of using nano powders as additives in grout mixtures were investigated in another experimental study conducted by Collepari et al. [12]. In this study, it has been shown that the increase in the rate of nano powder additives increases the cohesion value of the grout mixtures, while decreasing the setting time, segregation, and bleeding values. Moreover, some studies have shown that the addition of nano-alumina as an additive to cement-based grout has significant effects on the rheological properties, mechanical properties, and capillary water absorption capacity of these grouts [1,13]. These studies showed that higher ettringite contents can be produced during the early hydration process, due to the initial dissolution of nano alumina compared to other oxidized compounds.

Due to the colloidal nanoscale dimensions of nano powders, exposure to molecular electrical attraction may cause some problems such as agglomeration during mixing as an additive in grout mixtures. Due to the colloidal nano size of nano powders and the presence of nanoparticles adhering to each other, these materials cannot be homogeneously dispersed when added to grout mixes. Generally, this condition defined by the lack of effective dispersion method [14,15]. Dispersion and homogenization methods are usually tried to mix nano powders into cement-based grout in the most effective way [16,17]. If these methods are not applied, undesirable situations such as the accumulation of nano powders in grout mixes may occur and this situation generally reduces the viscosity of grout mixes. Therefore, the application of the ultra-sonification method is a useful technic to limit the agglomeration of nanomaterials and to provide more homogeneous distribution of nanomaterials in the slurry mixture [18,19].

Water-binder ratio (w/b) is one of the parameters that has the most important influence on the mechanical and fluidity properties of grout mixes. For this reason, the first parameter to be considered in the design of grout mixtures is known as determining the optimum water to binder ratio (w/b) for injection applications. With the increase of this ratio, the total water content of the grout mixes increases and as a result, the viscosity of the mixes decreases. This means that the fluidity and workability of grout mixes directly increase. This ratio generally varies in a wide range according to the application method in grout injections. While the w/b ratio for covering prestressed anchors usually ranges from 0.35 to 0.42, this ratio ranges from 0.5 to 1.5 for repair and strengthening of wall structures [20]. In addition, while this ratio is generally used between 0.5 and 1 for the sealing of cement slurries, it has been selected between 0.6 and 2 for jet grout applications in geotechnical works [21,22]. Studies conducted to date have shown that high w/b ratios negatively affect many mechanical behaviors of grout mixes. The increase in the w/b ratio during the preparation of the grout mixes decreases the hydration products required for the C-S-H gel formation of these samples, while increasing the bleeding rate for the fresh grout mixture. Therefore, some supplementary cementitious materials (SCMs) as mineral additives such as fly ash, silica fume, ground granulated blast furnace slag, metakaolin, bentonite and rice husk ash are usually used to minimize the adverse effects of high-water content in cement-based grouts. SCMs have been used as additives in cement-based grouts to keep properties such as resistance to chemical attack, control of hydration temperature and general durability of grout mixtures at the desired level and to eliminate the negativities observed in such properties [20–34]. The use of such mineral additives in the most effective mixing ratios has an important function in improving the various physical properties of grouts such as rheological, mechanical and workability properties [24]. There are very few mineral additives such as fly ash that not only increase the rheology, workability and long-term performance but also improve the durability properties of grouts [34,35].

Artificial neural networks (ANN), which started to be used in the middle of the 20th century, have become one of the mathematical tools that are frequently used by researchers due to their improved prediction performance [36]. ANNs, which are inspired by the biological structure of the human brain, have higher prediction performance compared to traditional tools, especially in modeling nonlinear functions [37]. In their study, Alyani et al. [38] applied single-pot hydrothermal synthesis for the growth of cobalt-doped TiO₂ nanosheets (Co-TNs) containing different amounts of cobalt on reduced graphene oxide surfaces (Co-TNs/rGO (x)). Synthesized nanocomposites were characterized by a series of analyzes including XRD, UV-Vis DRS, FESEM/EDX, elemental mapping, TEM, HRTEM and Raman spectroscopy, and the visible light degradation of Tetracycline antibiotic (TC) was investigated. An ANN model was used to estimate the photocatalytic removal of the tetracycline antibiotic. It was seen that the data obtained from the MLP network model with 14 neurons in its hidden layer gave optimum results. Xiang et al. [39] used the local ANN potential to study the Fx_E of the anatase type TiO₂ compound. They placed the flexoelectric TiO₂ coefficient according to the total energy of the double-field supercells predicted by the ANN potential for different shear-strain gradients. The value obtained because of the study is consistent with the previous experimental measured value. It is stated that the results show that the ANN potential is a suitable and efficient approach to examine Fx_E. To predict the rheological behavior of SAE50/MWCNTs-TiO₂ hybrid nano-lubricant, Chen et al. [40] obtained two separate data sets by curve fitting in power law and consistency indices, shear stress-shear rate diagrams. An optimal ANN was proposed to predict viscosity, and another ANN was proposed to predict the consistency index and the power law index. However, correlation was also developed using the same data set. The results obtained showed that for a precise estimation of the force law index, it is necessary to propose 6 equations, each corresponding to a temperature. The proposed correlations and comparisons between ANNs have also shown that ANNs are more useful than correlations. Çolak et al. [41] experimentally investigated the effect of high temperature on the flexural and compressive strength of mortars containing waste PET aggregates and proposed an ANN model. Mortar samples prepared in 5 different concentrations with waste PET aggregate substitution were heated up to 100, 150, 200, 250, 300 and 400°C and their flexural and compressive strengths were experimentally measured after waiting 1, 2 and 3 h at these temperatures. It was observed that the flexural strength and compressive strength values decreased with increasing temperature and PET aggregate amounts in all mixtures. It was seen that the ANN model developed can predict flexural and compressive strengths with an average error of -0.51%. Fedakar [42] has developed prediction models for the elasticity module using the ANN model. In the study, reliable empirical formulas for fine-grained soils are proposed using ANN. For this purpose, thousands of ANN models have been developed using long-term pavement performance and external datasets. The results showed that the constitutive models failed to predict the resilient modulus and the best resilient modulus estimates were obtained in the ANN-C9 model. Güllü et al. [43] presented a study on the application of artificial intelligence techniques, including radial-based neural network, MLP, generalized regression neural network, and adaptive neurofuzzy inference system. Prediction models were developed to predict the unconfined compressive strength of silty soil stabilized with bottom ash, jute fiber and steel fiber under different freeze-thaw cycles. The results showed that the predictions originating from all the artificial intelligence techniques used were ideally accurate. Kocabaş et al. [44] proposed a fuzzy genetic approach for modeling the critical submergence rate value. Channel flow velocity, inlet pipe velocity and porosity were used as inlet variables, and critical submergence rate as outlet variables. 44 datasets obtained through the experimental study were divided into two parts and 28 datasets were used for training and 16 datasets were used for testing the models. The experimental results were compared with the prediction values, and it was concluded that the models showed an ideal prediction performance.

For this reason, the use of nano powders as additives together with fly ash as mineral additives can provide significant contributions to the various physical, mechanical, fluidity and especially workability properties of cement-based grouts. The past studies mentioned above on grout mixtures have usually studied the use of nano silica, nano alumina, and nano calcium carbonate as nanomaterial. Furthermore, these studies generally were conducted with lower w/b ratios and focused on especially hardened features of grout mixture. As shown from the past works, any detailed experimental work has not been detected on how nano titanium oxide ($n\text{-TiO}_2$) will affect the workability of grout mixtures as fluidity properties at high w/b ratios. Also, no studies based on adding nano titanium oxide to fresh grout mix have been done on the workability properties of cement-based grouts combined with fly ash as a mineral additive. Therefore, the effects of nano titanium oxide ($n\text{-TiO}_2$) additions at different amounts by mass (0.0%, 0.3%, 0.6%, 0.9%, 1.2% and 1.5%) on the bleeding and the workability properties (mars cone flow time, mini slump spread diameter and plate cohesion) of cement-based grouts incorporated with fly ash as mineral additive at different constitutes (0%-for control purpose, 5%, 10%, 15%, 20%, 25% and 30%) were investigated by using a statistical modeling approach and analysis of experiments in this study.

2 Experimental Program

2.1 Materials

According to ASTM C150 standard CEM I-42.5R (Type-I) Portland cement (PC) and F-Class fly ash (FA) as supplementary cementitious materials (SCMs) were used in all experimental works. Fly ash was obtained from Isken Sugozy Termal Plant at Iskenderun-Turkey. Some physical and chemical properties of PC and FA used in the experimental study are presented in Table 1. All the properties given in Table 1 were obtained by these supplier companies.

Table 1: Some physical and chemical properties of Portland cement (PC) and FA

Chemical analysis (%)	CEM-I 42.5 R (Cement)	Fly ash (FA)
CaO	60.15	1.72
SiO ₂	20.46	62.21
Al ₂ O ₃	7.78	21.15
Fe ₂ O ₃	3.09	7.29
MgO	2.66	1.59
SO ₃	2.33	0.15
K ₂ O	0.82	2.12
Na ₂ O	0.22	0.94
TiO ₂	0.30	0.83
Physical analysis		
Loss on ignition	2.55	2.01
Specific gravity	3.10	2.33

Since particle size distribution of binders (cement and SCMs) is one of the most important parameters having a considerable effect on the workability properties of cement-based grouts, the particle size grain distribution curves of PC and FA used in this study were drawn by using laser scattering technique with the help of Master-sizer machine and all curves are shown in Fig. 1. According to Fig. 1, the gradation distributions of PC and FA are very close to each other. All particle grain sizes of FA are below

100-micron sizes, just like PC. The particle distribution of the binder admixture has considerable effects on the workability features of cement-based grouts.

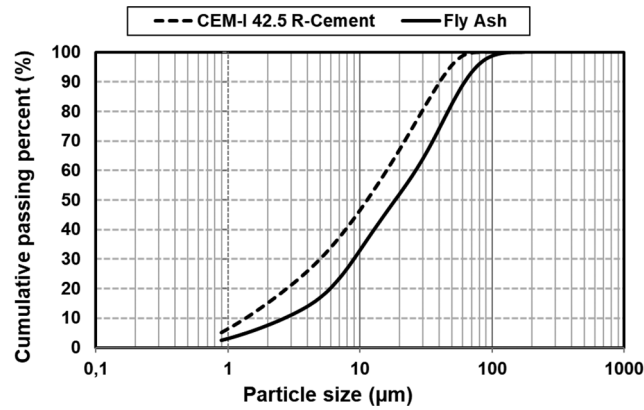


Figure 1: The particle size distribution curves of portland cement and fly ash (FA)

In this experimental work, nano titanium oxide ($n\text{-TiO}_2$) was used as Colloidal Nano Particular Powder (CNPP) additive. The SEM view of $n\text{-TiO}_2$ used in this work is shown in Fig. 2. Some elemental analysis and physical features of $n\text{-TiO}_2$ are presented in Tables 2 and 3. The nano titanium oxide ($n\text{-TiO}_2$) used in this work was supplied by a commercial firm called as Nanografi in Turkey, and these all properties were obtained by this firm.

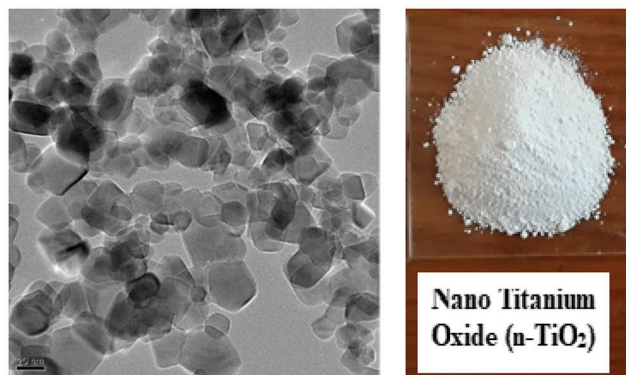


Figure 2: The SEM image of $n\text{-TiO}_2$ as nano additive used in this study

Table 2: Material analysis results of $n\text{-TiO}_2$ nanoparticle used in this experimental study

Elemental analysis	Na	Fe	K	Al
Nano Titanium Oxide ($n\text{-TiO}_2$) (%)	0.0076	0.0046	0.0085	0.0055

Table 3: Some physical properties of n-TiO₂ used in experimental study

Physical properties	n-TiO ₂
Purity (%)	99.6
Color	White
Average particle size (nm)	38
Specific surface area (m ² /g)	35
Mass density (g/cm ³)	0.4
Density (kg/m ³)	4100
Weight loss on drying (%)	1.2
Loss on ignition (%)	3.2
pH	5.5–6.5

2.2 Preparing the Fresh Mixtures and Mix Design

As commonly known that the w/b ratio has a remarkable influence on the workability properties of cement-based grouts. During the preparation of all grout mixes, the w/b ratio was set to 1, 0 in this study. To observe the effects of higher w/b ratio effect on the workability properties of grout mixes, this ratio was selected. The effects of nano titanium oxide (n-TiO₂) additions at various proportions by mass (0.0%, 0.3%, 0.6%, 0.9%, 1.2% and 1.5%) on workability of cement-based grouts replacement with fly ash as mineral additive at different contents (0%-for control purpose, 5%, 10%, 15%, 20%, 25% and 30%) were experimentally studied in this work. Table 4 presents mix design for the grout samples mixed with PC, FA and n-TiO₂. Total number of 42 grout mixes were obtained and tested as seen in this table.

Table 4: All mix ratios and mix design parameters used for preparing the grout samples

Mix ID	w/b	FA (%) [*]	PC (g) ^{**}	FA (g)	Water (g)	n-TiO ₂ (g)	Mix ID	w/b	FA (%)	PC (g)	FA (g)	Water (g)	n-TiO ₂ (g)
M1	1.0	-	1500	-	1500	-	M22	1.0	15	1275	225	1500	27
M2	1.0	-	1500	-	1500	9	M23	1.0	15	1275	225	1500	36
M3	1.0	-	1500	-	1500	18	M24	1.0	15	1275	225	1500	45
M4	1.0	-	1500	-	1500	27	M25	1.0	20	1200	300	1500	-
M5	1.0	-	1500	-	1500	36	M26	1.0	20	1200	300	1500	9
M6	1.0	-	1500	-	1500	45	M27	1.0	20	1200	300	1500	18
M7	1.0	5	1425	75	1500	-	M28	1.0	20	1200	300	1500	27
M8	1.0	5	1425	75	1500	9	M29	1.0	20	1200	300	1500	36
M9	1.0	5	1425	75	1500	18	M30	1.0	20	1200	300	1500	45
M10	1.0	5	1425	75	1500	27	M31	1.0	25	1125	375	1500	-
M11	1.0	5	1425	75	1500	36	M32	1.0	25	1125	375	1500	9
M12	1.0	5	1425	75	1500	45	M33	1.0	25	1125	375	1500	18
M13	1.0	10	1350	150	1500	-	M34	1.0	25	1125	375	1500	27
M14	1.0	10	1350	150	1500	9	M35	1.0	25	1125	375	1500	36

(Continued)

Mix ID	w/b	FA (%) [*]	PC (g) ^{**}	FA (g)	Water (g)	n-TiO ₂ (g)	Mix ID	w/b	FA (%)	PC (g)	FA (g)	Water (g)	n-TiO ₂ (g)
M15	1.0	10	1350	150	1500	18	M36	1.0	25	1125	375	1500	45
M16	1.0	10	1350	150	1500	27	M37	1.0	30	1050	450	1500	-
M17	1.0	10	1350	150	1500	36	M38	1.0	30	1050	450	1500	9
M18	1.0	10	1350	150	1500	45	M39	1.0	30	1050	450	1500	18
M19	1.0	15	1275	225	1500	-	M40	1.0	30	1050	450	1500	27
M20	1.0	15	1275	225	1500	9	M41	1.0	30	1050	450	1500	36
M21	1.0	15	1275	225	1500	18	M42	1.0	30	1050	450	1500	45

Failure to apply the effective dispersion method may cause some obstacles encountered during mixing of nano powders into cement-based grout samples [15]. To effectively obtain the most suitable dispersion conditions during mixing nano powders into cement-based grouts, effective dispersion method should be applied to samples [16,17]. Generally, the Ultra sonication method is applied to limit agglomeration and to provide a more homogeneous mixing of nano powders in the grout mix [18,19]. Therefore, to minimize n-TiO₂ precipitation in free water and to ensure homogeneous dispersion in water by removing these adhering nano powders from each other, the Ultra sonication method was applied in this study. The view of the Ultrasonicator test machine used in this work is shown in Fig. 3.

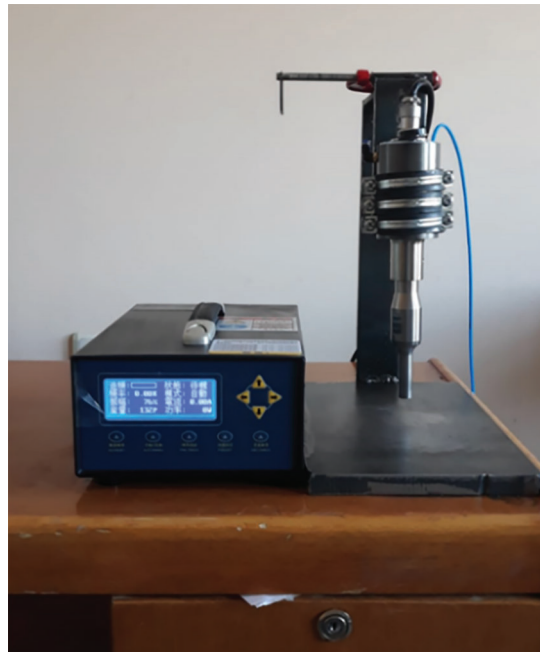


Figure 3: The image of the ultrasonicator used in the work

Ultra-sonication method was applied to the aqueous medium for 180 min as soon as preparing all the fresh grout mixes with mixing n-TiO₂ into 200 ml free water volume. After the distillation process was

completed, this aqueous mix was poured into cement-based grout mixes. Thus, nano titanium oxide ($n\text{-TiO}_2$) was added to the grout mixes without any clumping and non-uniform dispersion.

Similar mixing methodology was applied to obtain the grout samples at same conditions during preparing the mixtures. These samples were mixed by using a standard rotary laboratory mixer with a 5-liter volume capacity. To obtain the grout mixes, FA and PC as binder were first mixed with water for 1 min at 240 rpm speed. The mixer was then stopped and both binders were mixed by hand for 1 min to obtain a more homogeneous mixture. The samples were then mixed again with the mixer for 3 min at 240 rpm speed. In the last step, the aqueous medium containing $n\text{-TiO}_2$ and 200 ml of water prepared by Ultra sonication was added to the cement-based grout matrix and mixed with the mixer also for one more minute. During preparing samples and conducting tests, the ambient temperature and humidity were kept constant at $23 \pm 3^\circ\text{C}$ and 55%–65%, respectively.

2.3 Obtaining Workability and Bleeding Values

After the grout samples were mixed the workability and bleeding tests of the grout mixes were conducted. The preparation of the grout samples and the workability and bleeding tests on these samples were completed in an average of 12 min. While marsh cone flow, mini slump diameter and plate cohesion tests were being conducting in concept of workability tests, bleeding values of the grout mixtures were also measured as stability tests. The equipment views of marsh cone, mini slump cone and plate cohesion are detailly shown in [Fig. 4](#).



Figure 4: The view of workability tests conducted in the study

The mini slump diameter is generally estimated by the mini slump test defined as spreading of aqueous grout matrix on a flat plate. Height, bottom, and upper diameters of mini slump cone are 38 mm, 19 mm, and 57 mm, respectively [45]. The marsh cone flow test was applied as another workability test for grout mixes in this study. The main principles of this test based on measuring the elapsed time during flowing of fresh grout mix having a specific volume through this cone. This cone has 1500 ml volume, and its internal orifice diameter is 5 mm [22–23,25]. For all grout samples in this test, this swamp cone was filled with flow-plugged 1250 ml grout mixes. After the bottom outlet was opened, the time elapsed as soon as the flow of the grout started was measured and the total time for the 1000 ml grout sample to flow was recorded. To compare the results, only the flow time of water was tested, and the total flow time was measured as 24 s per 1000 ml volume. The last one as workability test is the Lombardi plate cohesion test completed in this study. The cohesion value, which is an important parameter directly related to the yield stress of grout mixtures, can be measured with the Lombardi plate cohesion test apparatus. Although there is no international standard defined for this test, it has been used in many past studies to define the cohesion of cement-based grouts [22–23,25,46]. The principle of this test can be defined as immersing a metallic plate to fresh grout samples and measuring the mass of grouts adhered on both side surfaces of the plate that has dimension of $300 \times 300 \times 3$ mm. Stability of cementitious grouts can be measured by controlling the precipitation of 1000 ml grout sample in a standard glass cylinder with a cross section diameter of 60 mm within 2 h (bleeding test) (see Fig. 5). The volumetric bleeding ($\Delta V/V$), described as the volume of clean water (ΔV) separated from the top of the suspension, is disunited by the original grout volume (i.e., $V = 1000$ ml) and saved to appraise the stability of a suspension. As stated in previous studies, if the bleeding rate that occurs after 2 h is below 10%, the mortar mixture is generally defined as a stable suspension [47,48]. The high sedimentation rate is characteristic of pure grout and has big practical outcome because if sedimentation of solids consists of during injection, the treated cavities and injection pipelines can become blocked, and the grout cannot flow any further.

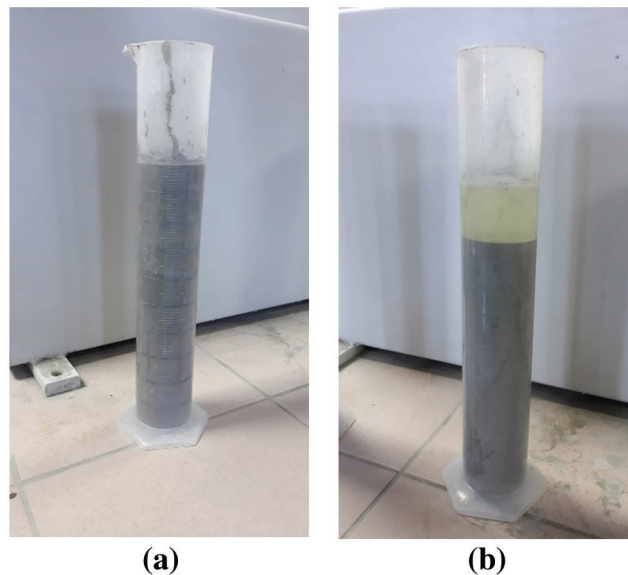


Figure 5: The bleeding test for stability control. (a) At the beginning of the test, (b) At the end of the test after 2 h

3 Development of the ANN Model

To predict the workability properties of cement-based grouts containing n-TiO₂ nanoparticle added fly ash, a feed-forward (FF) back-propagation (BP) multi-layer perceptron (MLP) ANN network model has been developed. MLP model, which is frequently preferred in ANNs, includes one input layer, at least one hidden layer and one output layer [49–51]. Input parameters to be used in the model are defined in the input layer. There is a computing element called a neuron in the hidden layer [52]. In the output layer, it is provided to obtain the predicted values. In the MLP network, each layer is linked to the next layer. The first step in the development of ANNs is to enter the data to be used for optimizing the data and training the model. After entering the data into the system, the training phase of the model is completed, and the forecast performance is analyzed. After determining the ANN model with the highest prediction performance, estimation values are obtained at the output layer. A flowchart for the development of an ANN model is shown in Fig. 6.

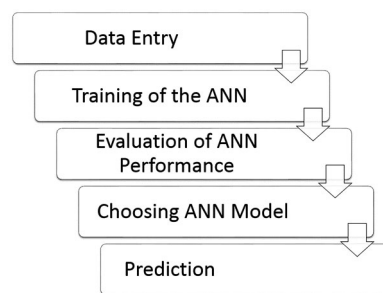


Figure 6: A flowchart for the development of an ANN model

Nanoparticle concentration (φ_{np}) and fly ash concentration (φ_{FA}) in the input layer of the ANN model, which has been developed to predict the workability properties of cement-based grouts containing n-TiO₂ nanoparticle added fly ash, Marsh cone flow time, mini slump spreading diameter and plate cohesion meter values are defined and Marsh cone flow time, mini slump spreading diameter and plate cohesion meter values are predicted in the output layer. The configuration structure of the developed MLP network model is shown in Fig. 7.

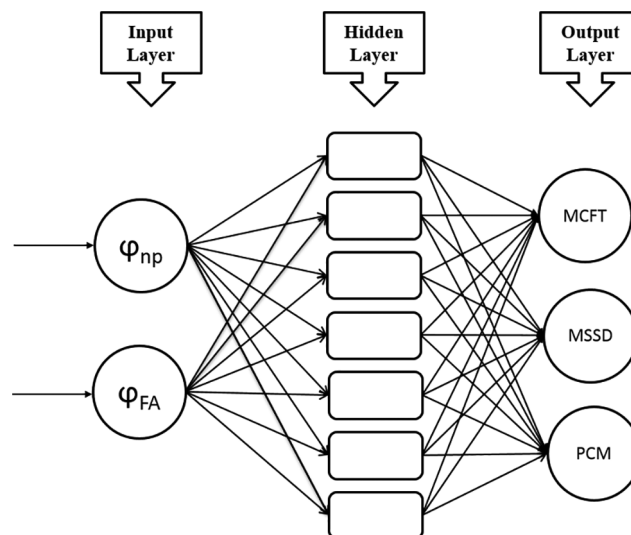


Figure 7: The configuration structure of the developed MLP network model

Ideally grouping and optimizing the data set used in the training of ANNs is an important parameter affecting the prediction performance of ANNs [53]. 70% (30) of the data used in the MLP network model, which has been developed with 42 experimental data, has been used for training, 15% (6) for validation and 15% (6) for the test phase. In data grouping, the model obtained from the literature and reported to provide high performance has been preferred [54–56]. There is no accepted model for determining the number of neurons to be used in the hidden layer of MLP networks [57,58]. For this reason, the predictive performances of the network models developed with different neuron numbers have been analyzed and the model with 5 neurons in the hidden layer has been preferred. The basic structure of the developed MLP network is shown in Fig. 8.

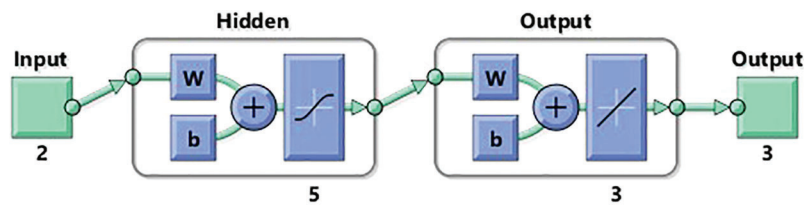


Figure 8: The basic structure of the developed MLP network

Levenberg-Marquardt training algorithm, one of the algorithms with high prediction performance, has been used as the training algorithm [59,60]. Tan-Sig and Purelin functions has been used as transfer function. The transfer functions used in ANN are given below [61,62]:

$$f(x) = \frac{1}{1 + \exp(-x)} \quad (1)$$

$$\text{purelin}(x) = x \quad (2)$$

Mean Squared Error (MSE), coefficient of determination (R) and error rate values have been chosen to analyze the predictive performance of ANNs. The mathematical formulas used to calculate performance parameters are given below [63]:

$$\text{MSE} = \frac{1}{N} \sum_{i=1}^N (X_{\text{exp}(i)} - X_{\text{ANN}(i)})^2 \quad (3)$$

$$R = \sqrt{1 - \frac{\sum_{i=1}^N (X_{\text{exp}(i)} - X_{\text{ANN}(i)})^2}{\sum_{i=1}^N (X_{\text{exp}(i)})^2}} \quad (4)$$

$$\text{Error Rate (\%)} = \left[\frac{X_{\text{exp}} - X_{\text{ANN}}}{X_{\text{exp}}} \right] \times 100 \quad (5)$$

4 Test Results and Discussions

In this experimental study, the workability and bleeding properties of cement-based grout mixes combined with FA and n-TiO₂ as colloidal nano powder were investigated, and some prediction models were developed with Artificial Neural Network (ANN). Marsh cone flow time, mini slump spreading diameter and Lombardi plate cohesion of the grout samples were measured, and all result are presented in Figs. 9–15.

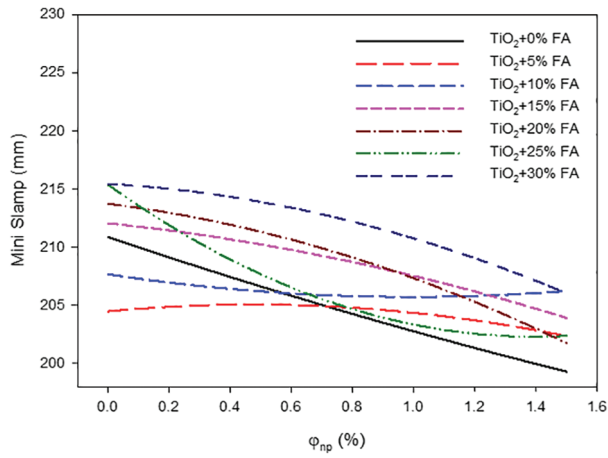


Figure 9: The mini slump diameter results obtained from the grout mixtures prepared by addition of n-TiO₂ and FA

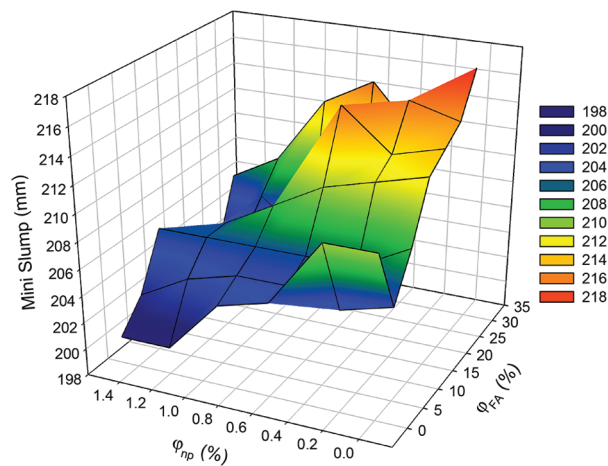


Figure 10: The mini slump diameter changes obtained from the grout mixtures prepared by addition of n-TiO₂ and FA in 3D view

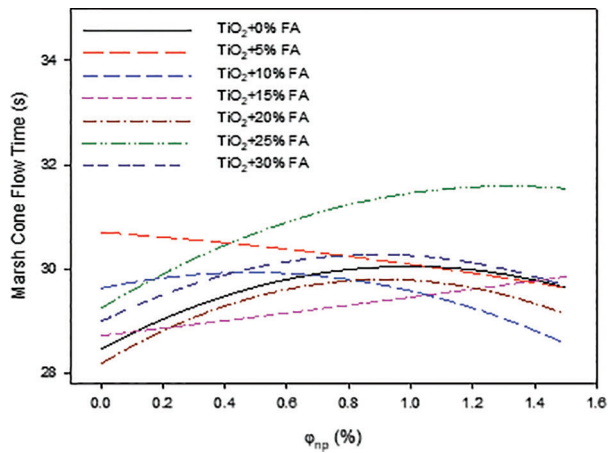


Figure 11: The marsh cone flow time changes of the grout samples prepared with addition of FA and n-TiO₂

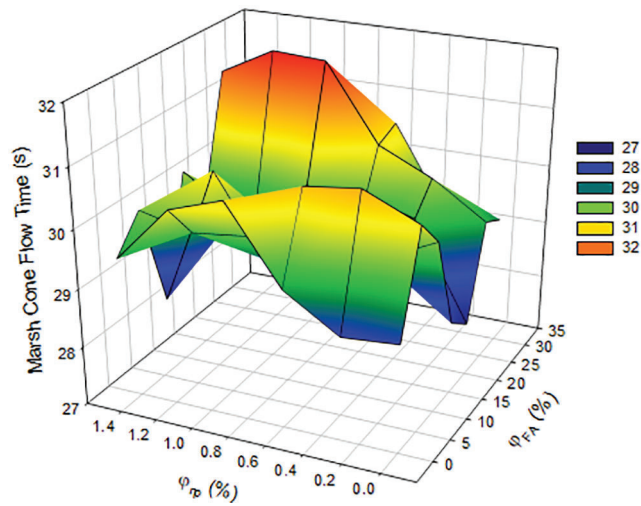


Figure 12: The marsh cone flow time changes of the grout samples prepared with addition of FA and n-TiO₂ in 3D view

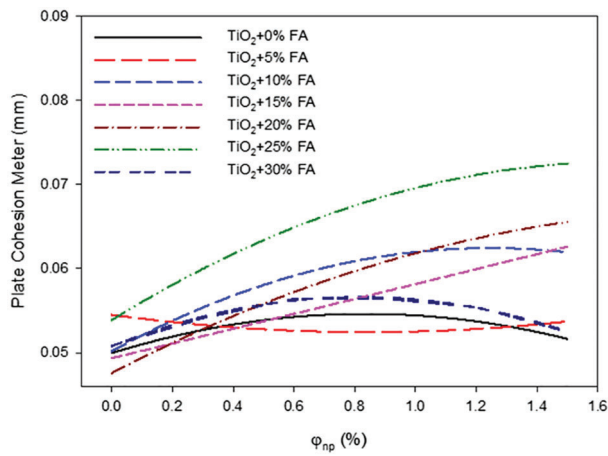


Figure 13: The plate cohesion changes of the grout samples prepared with addition of FA and n-TiO₂

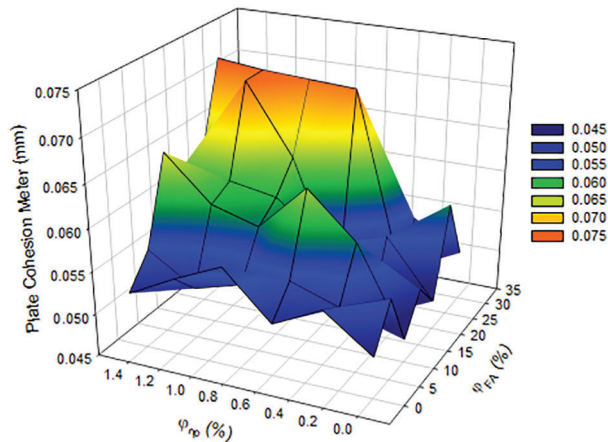


Figure 14: The plate cohesion meter changes of the grout samples prepared with addition of FA and n-TiO₂ in 3D view

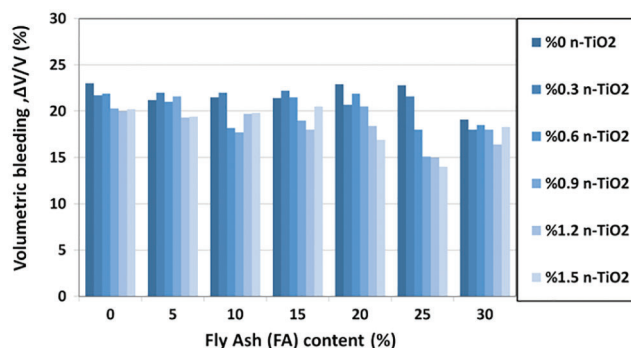


Figure 15: The volumetric bleeding changes of the grout samples prepared with addition of FA and n-TiO₂

When the results obtained from the samples prepared by addition of n-TiO₂ as CNPP is examined for mini slump test, an increase on mini slump spreading diameters can be observed with respect to rising amount of FA in the samples (see Fig. 9). The use of FA as a mineral additive in grout samples resulted in improvements in the workability behavior of the grout samples as expected [35,64–70].

On the other hand, increase amount of n-TiO₂ in the grout mixtures has made mini slump flow diameter of the samples slightly decrease. However, it cannot be mentioned about considerable reduction as can be seen in Fig. 10. The meaning of this slight reduction on the mini slump flow diameter of the samples can be explained as increase of cohesion in the sample and decrease of fluidity of the samples at a specific rate [9,10]. As can be seen in Table 3, the specific surface areas determined for n-TiO₂ measured as 35 m²/g. The slight decrease in the mini slump diameter values of the n-TiO₂ added grout mixes with the increase in the amount of nano material, and the fact that the mini slump diameter values of the n-TiO₂ added grout mixes are not significantly affected by the increase in the content of nanomaterials.

As in the mini slump spreading diameter experiment, it has been determined that the FA contribution increases the fluidity as the expected behavior, and this behavior causes a decrease in the marsh cone flow times for all mixtures (see Figs. 11 and 12). It was observed that the increase in the n-TiO₂ amount in grout matrix does not change the marsh cone flow time of mineral-added cement-based grouts so much in general trend. Although the effect seems to be less, the increase in n-TiO₂ content in grout mixtures caused a slight increase in the marsh cone flow time of the grout mixes. This increase can be explained as an increase in the cohesion value of the grout mixes due to the very low specific surface area of n-TiO₂. It can be also explained as n-TiO₂ have very high density as shown in Table 3. According to this table, its density is shown as 4100 kg/m³. Since n-TiO₂ is added by weight to the mixtures in the preparation of the grout samples, the volumetric effect of this nano powder in the mixture may affect the flow time changes.

As can be clearly seen from Figs. 11 and 12, it was determined that the mini slump spreading diameter and marsh cone flow time behave in harmony with each other with the addition of n-TiO₂ of the FA added grout mixtures.

As seen in Fig. 13, although the increase in the ratio of n-TiO₂ addition to the grout mixtures caused a small increase in the plate cohesion values of the samples, this increase cannot be considered as very remarkable increase on the fluidity features of these samples. This slight increase can be explained as an increase in the cohesion value of the grout mixes as same as marsh cone flow time and mini slump diameter values of the grout samples due to the very high specific surface area and very low density of n-TiO₂ [9–11]. This similar behavior was also observed in the past studies related with using of different nano powder as additive in grout mixtures [1–2,4,67].

In addition, as it is clearly seen from Fig. 14, FA substitution in the grout mixtures causes decrease of plate cohesion values of the samples. Although the increase in the nano titanium oxide additive increases the cohesion value, the FA additive limits this increase. In other words, the cohesion-increasing effect of nano titanium oxide is limited by adding FA [9–11]. This limitation in the cohesion values can be considered as an improvement in the workability behavior of the respective grout mixes [68–70].

Bleeding tests were carried out on the grout mixtures prepared within the scope of this experimental study. As a result of the experiments, bleeding values expressing the stability of the mixtures were determined. Volumetric bleeding ratios of all mixtures are shown in Fig. 15. As can be seen in Fig. 15, the bleeding values of all mixtures with and without n-TiO₂ remained below 900 ml (above 10% volumetric bleeding rate). In all FA additives, decreases in volumetric bleeding rates are observed due to the increase in the nano titanium oxide additive ratio. It has also been found that the FA additive causes a decrease in volumetric bleeding rates (see Fig. 15). It is clearly observed that the use of both FA and nano titanium oxide as additives causes an improvement in bleeding values in the cement-based grout mixes. As shown from Fig. 15, among all mixtures, the lowest volumetric bleeding rate (14%) was achieved at 25% FA and 1.5% n-TiO₂ additives. Bleeding rate above 10% is not a highly desirable situation in terms of the stability of the grouts [71]. As commonly known the fluidity of the mixtures is seriously affected by these bleeding behaviors. The reason why the bleeding values are so high can be explained by using the water-binding ratio ($w/b = 1$), which is considered high. This water-binder ratio is a value generally used in the permeation and jet grouting methods in ground improvement applications. The main purpose of selection this water to binder ratio in this study was considered as investigating these types of ground improvement applications.

Fig. 16 shows the training performance of the ANN model. It is seen that the MSE values in the graph are high at the beginning of the training phase of the ANN model and decrease in the later epochs. In the 4th epoch of the training phase, the optimum performance has been reached and the training process of the ANN model has been terminated with the achievement of the ideal performance values for all three data sets. This situation indicates that the training phase of the ANN model is ideally completed.

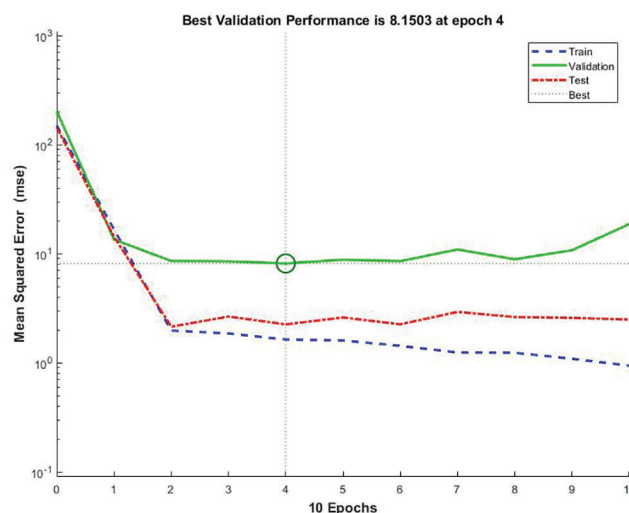


Figure 16: The training performance of the ANN model

The training status of ANN model can be seen in Fig. 17. It is seen that the gradient values decreased during the training period. However, the errors started after the 5th epoch and have been repeated 6 times. Error histogram showing the differences between the predicted values and target data obtained from the ANN model is given in Fig. 18. It is seen that the error values obtained for all three data sets are located close to the zero-error line and the numerical values are also low. The data obtained from the error histogram show that the training phase of the developed ANN model has been completed with low error values.

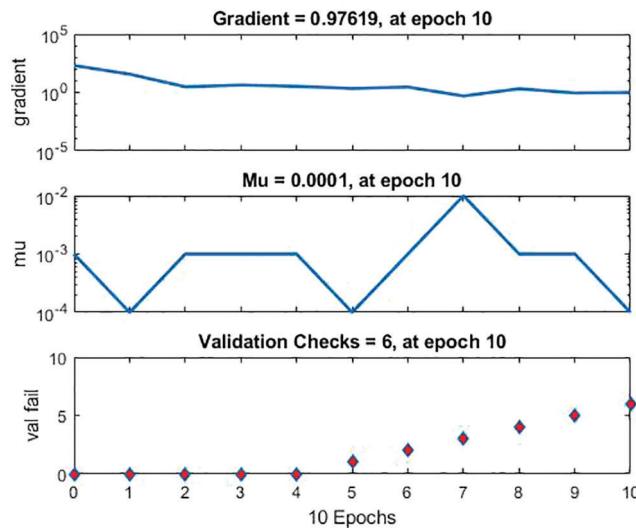


Figure 17: The training status of ANN model

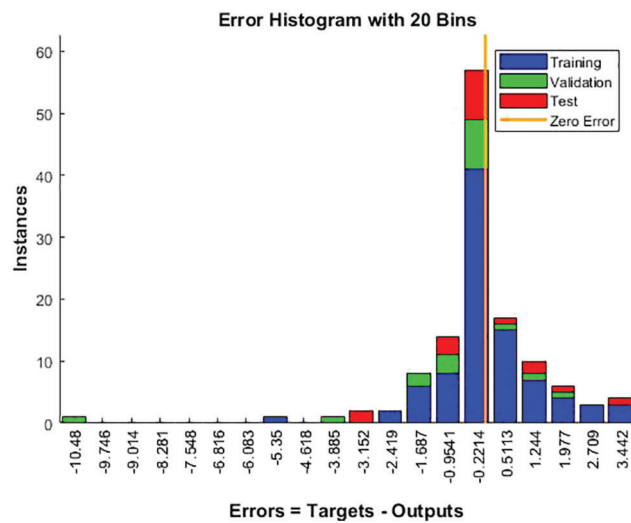


Figure 18: Error histogram of ANN model

In Fig. 19, the predicted values obtained from the ANN model and the experimental data, which are the target data, are shown for each data point. When the figure is considered, it is seen that the data points obtained from the ANN model and the data points representing the target data are located very close to each other. This proximity obtained at each point indicates that the predicted values obtained from the ANN model are in good agreement with the experimental data.

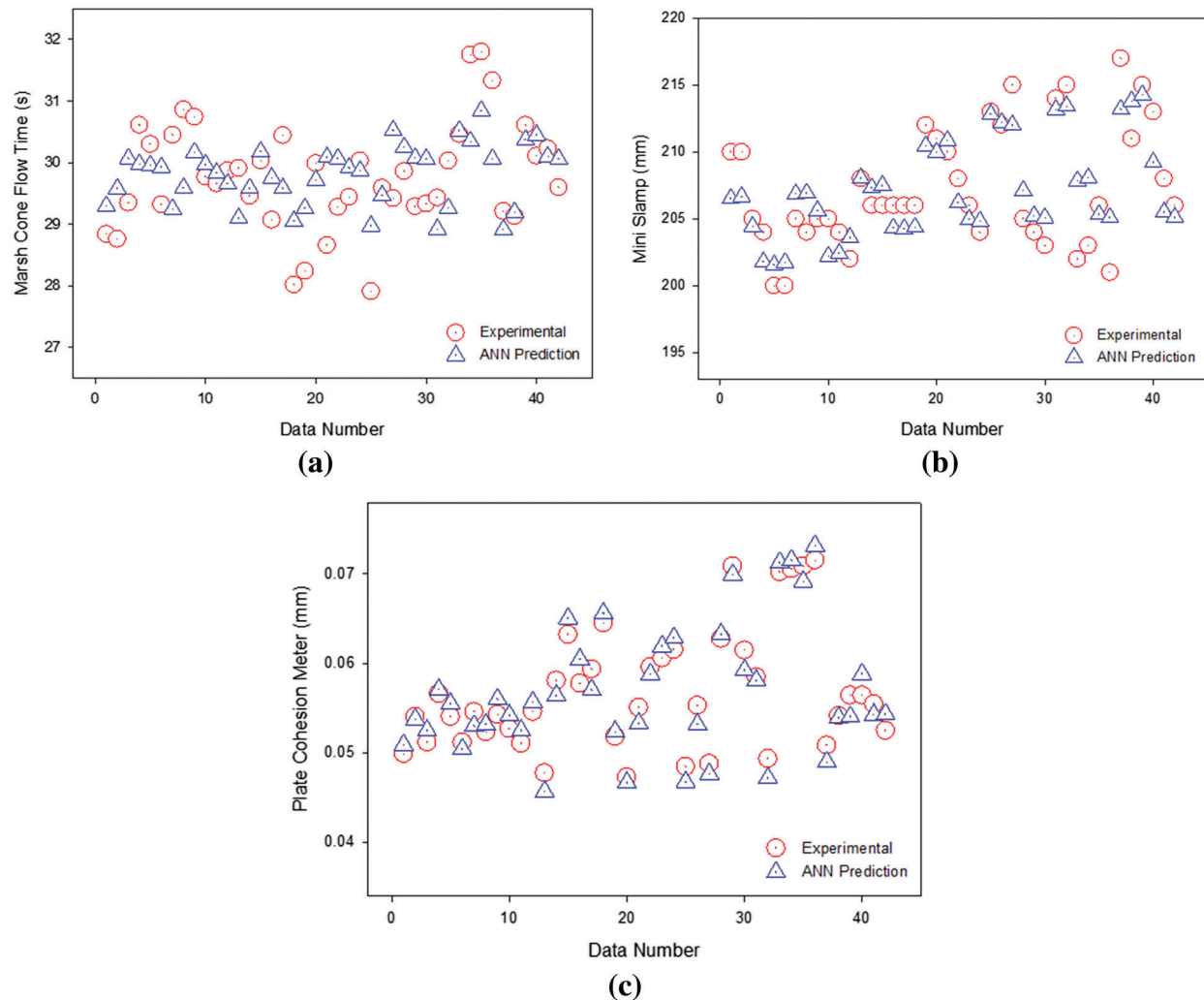


Figure 19: Predicted values obtained from the ANN model and the experimental data

Experimental data are located on the x-axis of Fig. 20, and ANN predictions are located on the y-axis. When the data points in the graphs are considered, it is seen that they are generally close to the equality line. This location of the data points shows that the error rates between ANN predictions and experimental data are at low values. In Fig. 21, the error rates between the predicted values obtained from the ANN model and the experimental data are given. When the error rates given separately for each data point used in the training of the MLP model are examined, it is seen that they are generally at low values and are located close to the zero-error line. However, it is also seen that the average error line also has a trend very close to the zero-error line. The ANN model can predict the marsh cone flow time value of cement-based grout containing n-TiO₂ nanoparticle added fly ash with an average error rate of -0.19% , the mini slump spreading diameter value with an average error rate of 0.04% and the plate cohesion meter value with an average error rate of 0.15% . Performance parameters of the developed ANN model are given in Table 5.

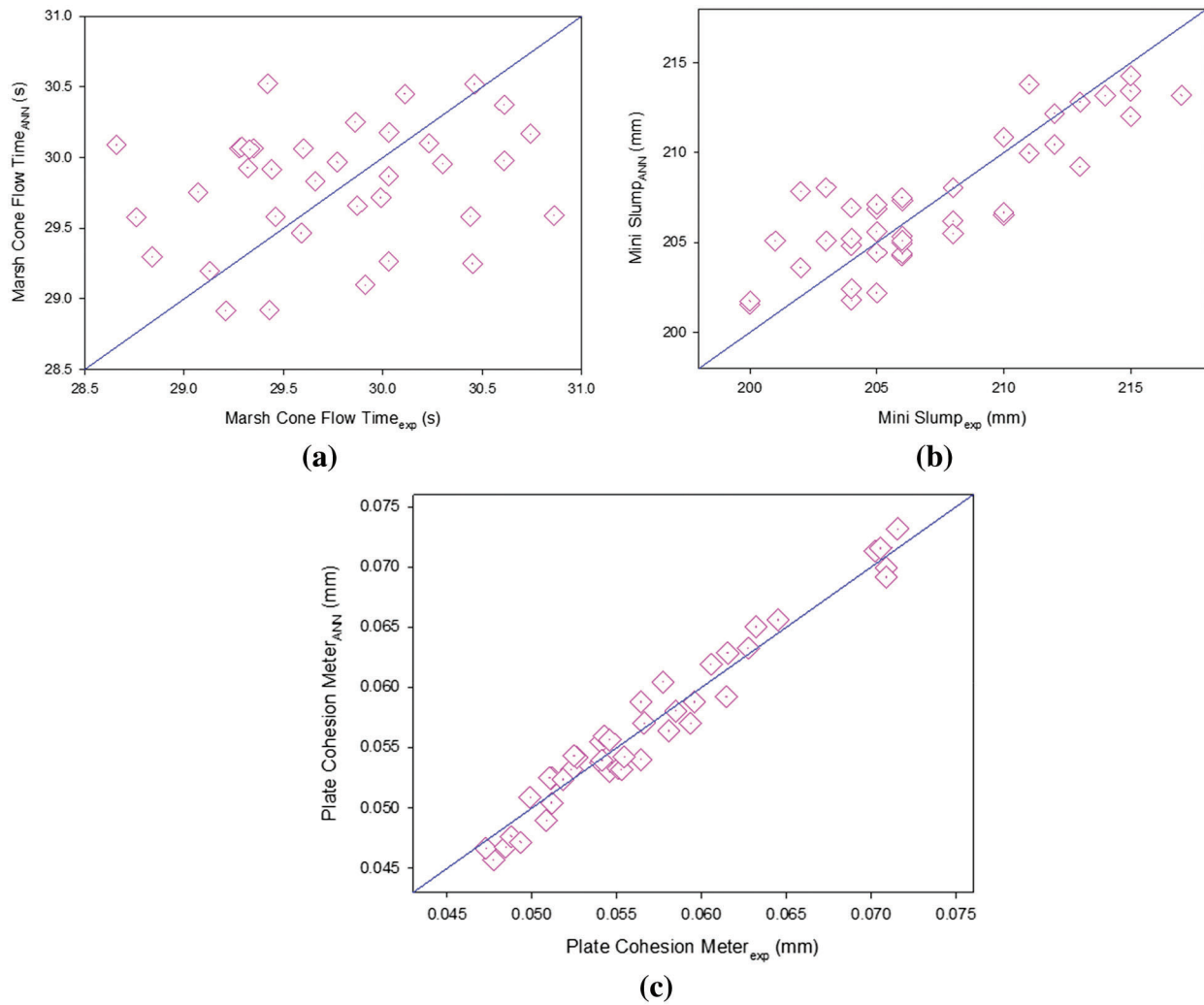


Figure 20: Experimental data vs. ANN prediction

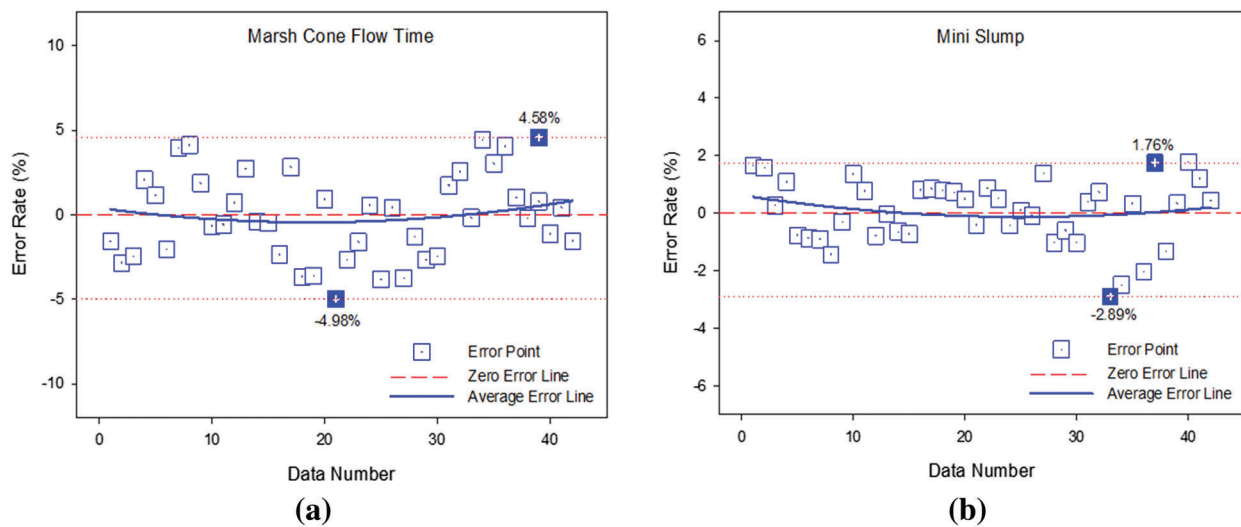


Figure 21: (Continued)

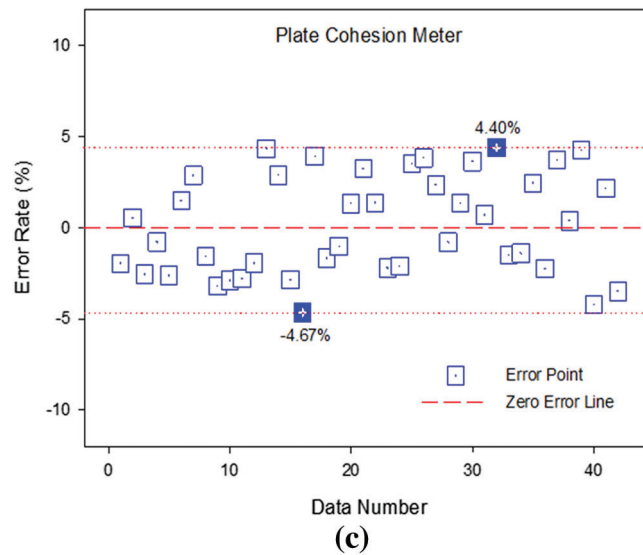


Figure 21: Error rates for ANN model

Table 5: Performance parameters of ANN model

	MSE	R	Error rate (%)
Marsh cone flow time	3.82E-02	0.99984	-0.19
Mini slump spreading diameter	2.51E-02		0.04
Plate cohesion meter	3.28E-02		0.15

5 Conclusions

Marsh cone flow time, mini slump spreading diameter and plate cohesion meter values have been measured experimentally to analyze the workability properties of cement-based grouts containing n-TiO₂ nanoparticle added fly ash. The use of FA as a mineral additive in grout samples resulted in improvements in the workability behavior of the grout samples as expected. On the other hand, increase amount of n-TiO₂ in the grout mixtures has made mini slump flow diameter of the samples slightly decrease. The FA contribution behavior causes a decrease in the marsh cone flow times for all mixtures. The increase in the n-TiO₂ amount in grout matrix does not change the marsh cone flow time of mineral-added cement-based grouts so much in general trend. Although the increase in the ratio of n-TiO₂ addition to the grout mixtures caused a small increase in the plate cohesion values of the samples, this increase cannot be considered as very remarkable increase on the fluidity features of these samples. The FA additive causes a decrease in volumetric bleeding rates. It is clearly observed that the use of both FA and nano titanium oxide as additives causes an improvement in bleeding values in the cement-based grout mixes.

Using the experimental data obtained, an ANN model has been developed. Nanoparticle concentration (ϕ_{np}) and fly ash concentration (ϕ_{FA}) input parameters have been defined in the input layer of the MLP network, which has been developed with a total of 42 experimental data, and Marsh cone flow time, mini slump spreading diameter and plate cohesion meter values have been predicted in the output layer. In the hidden layer, 30 of the data used in the development of the ANN model, which has been developed with 5 neurons, have been used for training, 6 for validation and 6 for testing. The predictive values obtained

from the ANN model have been compared with the experimental data, which are the target data, and the predictive performance of the ANN model has been analyzed. The findings obtained in the study showed that the developed ANN model can predict Marsh cone flow time, mini slump spreading diameter and plate cohesion meter values with very low error rates and high accuracy of cement-based grouts containing n-TiO₂ nanoparticle added fly ash.

Acknowledgement: The authors would like to thank TUBITAK for its great support.

Funding Statement: This study was funded by The Scientific and Technological Research Council of Turkey-TUBITAK [Grant No. 219M522].

Conflicts of Interest: The authors declare that they have no conflicts of interest to report regarding the present study.

References

1. Peng, Y., Ma, K., Long, G., Xie, Y. (2019). Influence of nano-SiO₂, nano-CaCO₃ and nano-Al₂O₃ on rheological properties of cement–Fly Ash paste. *Materials*, 12, 2598. DOI 10.3390/ma1216259.
2. Rashad, A. M. (2013). A synopsis about the effect of nano-Al₂O₃, nano-Fe₂O₃, nano-Fe₃O₄ and nano-clay on some properties of cementitious materials–A short guide for civil engineer. *Materials and Design*, 52, 143–157. DOI 10.1016/j.matdes.2013.05.035.
3. Song, S. Q., Jiang, L. H., Jiang, S. B., Yan, X. C., Xu, N. (2018). The mechanical properties and electrochemical behavior of cement paste containing nano-MgO at different curing temperature. *Construction and Building Materials*, 164, 663–671. DOI 10.1016/j.conbuildmat.2018.01.011.
4. Singh, L. P., Bhattacharyya, S. K., Ahalawat, S. (2012). Preparation of size controlled silica nano particles and Its functional role in cementitious system. *Journal of Advanced Concrete Technology*, 10, 345–352. DOI 10.3151/jact.10.345.
5. Madani, H., Bagheri, A., Parhizkar, T. (2012). The pozzolanic reactivity of monodispersed nanosilica hydrosols and their influence on the hydration characteristics of Portland cement. *Cement and Concrete Research*, 42, 1563–1570. DOI 10.1016/j.cemconres.2012.09.004.
6. Bjornstrom, J., Martinelli, A., Matic, A., Borjesson, L., Panas, I. (2004). Accelerating effects of colloidal nano-silica for beneficial calcium-silicate-hydrate formation in cement. *Chemical Physics Letters*, 392, 242–324. DOI 10.1016/j.cplett.2004.05.071.
7. Nazari, A., Riahi, S. (2011). The effects of SiO₂ nanoparticles on physical and mechanical properties of high strength compacting concrete. *Composite Part B: Engineering*, 42, 570–578. DOI 10.1016/j.compositesb.2010.09.025.
8. Hou, P. K., Kawashima, S., Kong, D. Y., Corr, D. J., Qian, J. S. et al. (2013). Modification effects of colloidal nano SiO₂ on cement hydration and its gel property. *Composite Part B: Engineering*, 45, 440–448. DOI 10.1016/j.compositesb.2012.05.056.
9. Zabihi, N., Ozkul, M. H. (2018). The fresh properties of nano silica incorporating polymer-modified cement pastes. *Construction and Building Materials*, 168, 570–579. DOI 10.1016/j.conbuildmat.2018.02.084.
10. Balapour, M., Joshaghani, A., Althoey, F. (2018). Nano-SiO₂ contribution to mechanical, durability, fresh and microstructural characteristics of concrete: A review. *Construction and Building Materials*, 181, 27–41. DOI 10.1016/j.conbuildmat.2018.05.266.
11. Ouyang, J., Han, B. G., Chen, G. Z., Zhao, L. Z., Ou, J. P. (2018). A viscosity prediction model for cement paste with nano-SiO₂ particles. *Construction and Building Materials*, 185, 293–301. DOI 10.1016/j.conbuildmat.2018.07.070.
12. Collepardi, S., Borsoi, A., Olagot, J. J. O., Troli, R., Collepardi, M. et al. (2005). Influence of nano-sized mineral additions on performance of SCC. *Proceedings of the 6th International Congress, Global Construction, Ultimate Concrete Opportunities*, Dundee.

13. Oltulu, M., Sahin, R. (2013). Effect of nano-SiO₂, nano-Al₂O₃ and nano-Fe₂O₃ powders on compressive strengths and capillary water absorption of cement mortar containing fly ash: A comparative study. *Energy and Buildings*, 58, 292–301. DOI 10.1016/j.enbuild.2012.12.014.
14. Liu, X. Y., Chen, L., Liu, A. H., Wang, X. R. (2012). Effect of nano-CaCO₃ on properties of cement paste. *Energy Procedia*, 16, 991–996. DOI 10.1016/j.egypro.2012.01.158.
15. Meng, W., Khayat, K. H. (2018). Effect of graphite nanoplatelets and carbon nanofibers on rheology, hydration, shrinkage, mechanical properties, and microstructure of UHPC. *Cement and Concrete Research*, 105, 64–71. DOI 10.1016/j.cemconres.2018.01.001.
16. Metaxa, Z. S., Konsta-Gdoutos, M., Shah, S. P. (2010). Carbon nanofiber-reinforced cement-based materials. *Transportation Research Record*, 2142, 114–118. DOI 10.3141/2142-17.
17. Kirgiz, M. S. (2015). Advance treatment by nanographite for portland pulverised fly ash cement (the class F) systems. *Composite Part B*, 82, 59–71. DOI 10.1016/j.compositesb.2015.08.003.
18. Konsta-Gdoutos, M. S., Metaxa, Z. S., Shah, S. P. (2010). Highly dispersed carbon nanotube reinforced cement-based materials. *Cement and Concrete Research*, 40 (7), 1052–1059. DOI 10.1016/j.cemconres.2010.02.015.
19. Peyvandi, A., Soroushian, P., Abdol, N., Balachandra, A. M. (2013). Surface-modified graphite nanomaterials for improved reinforcement efficiency in cementitious paste. *Carbon*, 63, 175–186. DOI 10.1016/j.carbon.2013.06.069.
20. Woodward, R. J., Miller, E. (1990). Grouting post-tensioned concrete bridges: The prevention of voids. *Highway Transport*, 37(6), 9–17.
21. Moseley, M. P. (1993). *Ground improvement*. Florida: Blackie Academic and Professional.
22. Cry, M., Legrand, C., Mouret, M. (2000). Study of the shear thickening effect of superplasticizers on the rheological behaviour of cement pastes containing or not mineral additives. *Cement and Concrete Research*, 30, 1477–1483. DOI 10.1016/S0008-8846(00)00330-6.
23. Celik, F., Canakci, H. (2015). An investigation of rheological properties of cement-based grout mixed with rice husk ash (RHA). *Construction and Building Materials*, 91, 187–194. DOI 10.1016/j.conbuildmat.2015.05.025.
24. Sonebi, M., Bassuoni, M. T., Kwasny, J., Amanuddin, A. K. (2014). Effect of nanosilica on rheology, fresh properties, and strength of cement-based grouts. *Journal of Materials in Civil Engineering*, 27(4), 04014145. DOI 10.1061/(ASCE)MT.1943-5533.0001080.
25. Celik, F., Akcuru, O. (2020). Rheological and workability effects of bottom ash usage as a mineral additive on the cement-based permeation grouting method. *Construction and Building Materials*, 263, 120186. DOI 10.1016/j.conbuildmat.2020.120186.
26. Sonebi, M. (2006). Rheological properties of grouts with viscosity modifying agents as diutan gum and welan gum incorporating pulverised fly ash. *Cement and Concrete Research*, 36(9), 1609–1618. DOI 10.1016/j.cemconres.2006.05.016.
27. Yamamoto, Y., Kobayashi, S. (1986). Effect of temperature on the properties of superplasticized concrete. *ACI Materials Journal*, 83(1), 80–87.
28. Golaszewski, J., Szwabowski, J. (2004). Influence of superplasticizer on rheological behaviour of fresh cement mortars. *Cement and Concrete Research*, 34(2), 235–248. DOI 10.1016/j.cemconres.2003.07.002.
29. Jolicoeur, C., Sharman, J., Otis, N., Lebel, A., Simard, M. A. et al. (1997). The influence of temperature on the rheological properties of superplasticized cement pastes. *5th CANMET/ACI International Conference on Superplasticizers and Other Chemical Admixtures in Concrete*, vol. 173, pp. 379–406. Rome, Italy.
30. Petit, J. Y., Wirquin, E., Duthoit, B. (2005). Influence of temperature on the yield value of highly flowable micromortars made with sulfonate-based superplasticizer. *Cement and Concrete Research*, 35(2), 256–266. DOI 10.1016/j.cemconres.2004.04.025.
31. Petit, J. Y., Khayat, K., Wirquin, E. (2009). Coupled effect of time and temperature on variations of yield value of highly flowable mortar. *Cement and Concrete Research*, 39(3), 165–170. DOI 10.1016/j.cemconres.2008.12.007.
32. Sonebi, M., Lachemi, M., Hossain, K. M. A. (2013). Optimisation of rheological parameters and mechanical properties of superplasticised cement grouts containing metakaolin and viscosity modifying admixture. *Construction and Building Materials*, 38(1), 126–138. DOI 10.1016/j.conbuildmat.2012.07.102.

33. Sonebi, M. (2010). Optimization of cement grouts containing silica fume and viscosity modifying admixture. *Journal of Materials in Civil Engineering*, 22(4), 1–11. DOI 10.1061/(ASCE)MT.1943-5533.0000026.
34. Celik, F. (2019). The observation of permeation grouting method as soil improvement technique with different grout flow models. *Geomechanics and Engineering*, 17 (4), 367–374. DOI 10.12989/gae.2019.17.4.367.
35. Sonebi, M. (2002). Experimental design to optimize high-volume of fly ash grout in the presence of welan Gum and super plasticizer. *Materials and Structures*, 35(250), 373–380. DOI 10.1617/13752.
36. Bas, E., Uslu, V. R., Egrioglu, E. (2016). Robust learning algorithm for multiplicative neuron model artificial neural networks. *Expert Systems with Applications*, 56, 80–88. DOI 10.1016/j.eswa.2016.02.051.
37. Vakili, M., Khosrojerdi, S., Aghajannezhad, P., Yahyaei, M. (2017). A hybrid artificial neural network-genetic algorithm modeling approach for viscosity estimation of graphene nanoplatelets nanofluid using experimental data. *International Communications in Heat and Mass Transfer*, 82, 40–48. DOI 10.1016/j.icheatmasstransfer.2017.02.003.
38. Alyani, S. J., Pirbazari, A. E., Khalilsaraei, F. E., Kolar, N. A., Gilani, N. (2019). Growing Co-doped TiO₂ nanosheets on reduced graphene oxide for efficient photocatalytic removal of tetracycline antibiotic from aqueous solution and modeling the process by artificial neural network. *Journal of Alloys and Compounds*, 799, 169–182. DOI 10.1016/j.jallcom.2019.05.175.
39. Xiang, L., Zeng, X., Huang, X., Li, G. (2020). The application of artificial neural-network potentials for flexoelectricity: Performance for anatase-type TiO₂. *Physics Letters A*, 384, 126217. DOI 10.1016/j.physleta.2019.126217.
40. Chen, Z., Ashkezari, A. Z., Tlili, I. (2020). Applying artificial neural network and curve fitting method to predict the viscosity of SAE50/MWCNTs-TiO₂ hybrid nanolubricant. *Physica A: Statistical Mechanics and its Applications*, 549, 123946. DOI 10.1016/j.physa.2019.123946.
41. Çolak, A. B., Akçaözöğlü, K., Akçaözöğlü, S., Beller, G. (2021). Artificial intelligence approach in predicting the effect of elevated temperature on the mechanical properties of PET aggregate mortars: An experimental study. *Arabian Journal for Science and Engineering*, 46(5), 4867–4881. DOI 10.1007/s13369-020-05280-1.
42. Fedakar, HI (2021). Developing New empirical formulae for the resilient modulus of fine-grained subgrade soils using a large long-term pavement performance dataset and artificial neural network approach. *Transportation Research Record: Journal of the Transportation Research Board*, 2676(4). DOI 10.1177/036119812111057054.
43. Güllü, H., Fedakar, HI (2017). On the prediction of unconfined compressive strength of silty soil stabilized with bottom ash, jute and steel fibers via artificial intelligence. *Geomechanics and Engineering*, 12, 441–464. DOI 10.12989/gae.2017.12.3.441.
44. Kocabaş, F., Ünal, B., Ünal, S., Fedakar, HI, Gemici, E. (1980). Fuzzy genetic approach for modeling of the critical submergence of an intake. *Neural Computing and Applications*, 23, 73–82. DOI 10.1007/s00521-012-1241-6.
45. Kantro, D. L. (1980). Influence of water reducing admixtures on properties of cement paste a miniature slump test. *Cement Concrete and Aggregates*, 2(2), 95–102. DOI 10.1520/CCA10190J.
46. Weaver, K. (1991). *Dam foundation grouting*. USA: American Society of Civil Engineers, ASCE Press, DOI 10.1061/9780784407646.
47. Kauschinger, L. J., Perry, E. R., Hankour, R. (1992). Methods to estimate composition of jet grout bodies. In: *Grouting, soil improvement and geosynthetics*, vol. 30, 194–205. New Orleans, Louisiana, USA.
48. Celik, F., Canakci, H. (2020). Examination of the mechanical properties and failure pattern of soilcrete mixtures modified with rice husk ash. *European Journal of Environmental and Civil Engineering*, 24, 1245–1260. DOI 10.1080/19648189.2018.1458656.
49. Çolak, A. B. (2020). Developing optimal artificial neural network (ANN) to predict the specific heat of water based yttrium oxide (Y₂O₃) nanofluid according to the experimental data and proposing new correlation. *Heat Transfer Research*, 51(17), 1565–1586. DOI 10.1615/HeatTransRes.2020034724.
50. Canakci, A., Ozsahin, S., Varol, T. (2012). Modeling the influence of a process control agent on the properties of metal matrix composite powders using artificial neural networks. *Powder Technology*, 228, 26–35. DOI 10.1016/j.powtec.2012.04.045.

51. Vaferi, B., Eslamloueyan, R., Ayatollahi, S. (2011). Automatic recognition of oil reservoir models from well testing data by using multi-layer perceptron networks. *Journal of Petroleum Science and Engineering*, 77, 254–262. DOI 10.1016/j.petrol.2011.03.002.
52. Ahmadloo, E., Azizi, S. (2016). Prediction of thermal conductivity of various nanofluids using artificial neural network. *International Communications in Heat and Mass Transfer*, 74, 69–75. DOI 10.1016/j.icheatmasstransfer.2016.03.008.
53. Çolak, A. B. (2021). An experimental study on the comparative analysis of the effect of the number of data on the error rates of artificial neural networks. *International Journal of Energy Research*, 45(1), 478–500. DOI 10.1002/er.5680.
54. Esmaeilzadeh, F., Teja, A. S., Bakhtyari, A. (2020). The thermal conductivity, viscosity, and cloud points of bentonite nanofluids with n-pentadecane as the base fluid. *Journal of Molecular Liquids*, 300, 112307. DOI 10.1016/j.molliq.2019.112307.
55. Barati-Harooni, A., Najafi-Marghmaleki, A. (2016). An accurate RBF-NN model for estimation of viscosity of nanofluids. *Journal of Molecular Liquids*, 224, 580–588. DOI 10.1016/j.molliq.2016.10.049.
56. Rostamian, S. H., Biglari, M., Saedodin, S., Esfe, M. H. (2017). An inspection of thermal conductivity of CuO-SWCNTs hybrid nanofluid versus temperature and concentration using experimental data, ANN modeling and new correlation. *Journal of Molecular Liquids*, 231, 364–369. DOI 10.1016/j.molliq.2017.02.015.
57. Bonakdari, H., Zaji, A. H. (2016). Open channel junction velocity prediction by using a hybrid self-neuron adjustable artificial neural network. *Flow Measurement and Instrumentation*, 49, 46–51. DOI 10.1016/j.flowmeasinst.2016.04.003.
58. Çolak, A. B., Güzel, T., Yıldız, O., Özer, M. (2021). An experimental study on determination of the shottky diode current-voltage characteristic depending on temperature with artificial neural network. *Physica B: Condensed Matter*, 608, 412852. DOI 10.1016/j.physb.2021.412852.
59. Ali, A., Abdulrahman, A., Garg, S., Maqsood, K., Murshid, G. (2019). Application of artificial neural networks (ANN) for vapor-liquid-solid equilibrium prediction for CH₄-CO₂ binary mixture. *Greenhouse Gases*, 9, 67–78. DOI 10.1002/ghg.1833.
60. Kareem, A., Shariff, F. A., Ullah, A. M., Garg, S., Dreisbach, S. et al. (2017). Experimental and neural network modeling of partial uptake for a carbon dioxide/methane/water ternary mixture on 13X zeolite. *Energy Technology*, 5, 1373–1391. DOI 10.1002/ente.201600688.
61. Vafaei, M., Afrand, M., Sina, N., Kalbasi, R., Sourani, F. et al. (2017). Evaluation of thermal conductivity of MgO-MWCNTs/EG hybrid nanofluids based on experimental data by selecting optimal artificial neural networks. *Physica E: Low-Dimensional Systems and Nanostructures*, 85, 90–96. DOI 10.1016/j.physe.2016.08.020.
62. Akhgar, A., Toghraie, D., Sina, N., Afrand, M. (2019). Developing dissimilar artificial neural networks (ANNs) to prediction the thermal conductivity of MWCNT-TiO₂/Water-ethylene glycol hybrid nanofluid. *Powder Technology*, 355, 602–610. DOI 10.1016/j.powtec.2019.07.086.
63. Çolak, A. B., Yıldız, O., Bayrak, M., Tezekici, B. S. (2020). Experimental study for predicting the specific heat of water based Cu-Al₂O₃ hybrid nanofluid using artificial neural network and proposing new correlation. *International Journal of Energy Research*, 44(9), 7198–7215. DOI 10.1002/er.5417.
64. Çinar, M., Karpuzcu, M., Çanakci, H. (2019). Effect of waste marble powder and fly ash on the rheological characteristics of cement based grout. *Civil Engineering Journal*, 5(4), 777–788. DOI 10.28991/cej-2019-03091287.
65. Çinar, M., Karpuzcu, M., Çanakci, H. (2020). The measurement of fresh properties of cement-based grout containing waste marble powder. *Measurement*, 150, 106833. DOI 10.1016/j.measurement.2019.07.061.
66. Çinar, M., Çelik, F., Çanakci, H., Nassani, D. E. (2017). Fresh properties of cementitious grout with rice husk powder. *Arabian Journal for Science and Engineering*, 42(9), 3819–3827. DOI 10.1007/s13369-017-2467-5.
67. Senff, L., Labrincha, J. A., Ferreira, V. M., Hotza, D., Repette, W. L. (2009). Effect of nano-silica on rheology and fresh properties of cement pastes and mortars. *Construction and Building Materials*, 23(7), 2487–2491. DOI 10.1016/j.conbuildmat.2009.02.005.

68. Guo, Y., Zhao, P., Zhang, Q., Liu, R., Zhang, L. et al. (2019). Investigation of the mechanism of grout penetration in intersected fractures. *Fluid Dynamics & Materials Processing*, 15(4), 321–342. DOI 10.32604/fdmp.2019.07844.
69. Zhai, Y., Li, L., Xuan, Z., Ma, M., Wang, H. (2023). Experimental performance evaluation and artificial-neural-network modeling of ZnO-CuO/EG-W hybrid nanofluids. *Fluid Dynamics & Materials Processing*, 18(3), 629–646. DOI 10.32604/fdmp.2022.017485.
70. Jalali, H., Abbassi, H. (2019). Analysis of the influence of viscosity and thermal conductivity on heat transfer by Al₂O₃-water nanofluid. *Fluid Dynamics & Materials Processing*, 15(3), 253–270. DOI 10.32604/fdmp.2019.03896.
71. Deere, D. U. (1982). Cement-bentonite grouting for dams. *Proceedings of ASCE Specialty Conference on Grouting in Geotechnical Engineering*, pp. 279–300. New Orleans, USA.